Volume 61
Number 54
11 July 2025
Pages 9723–9984

ChemComm

Chemical Communications

rsc.li/chemcomm

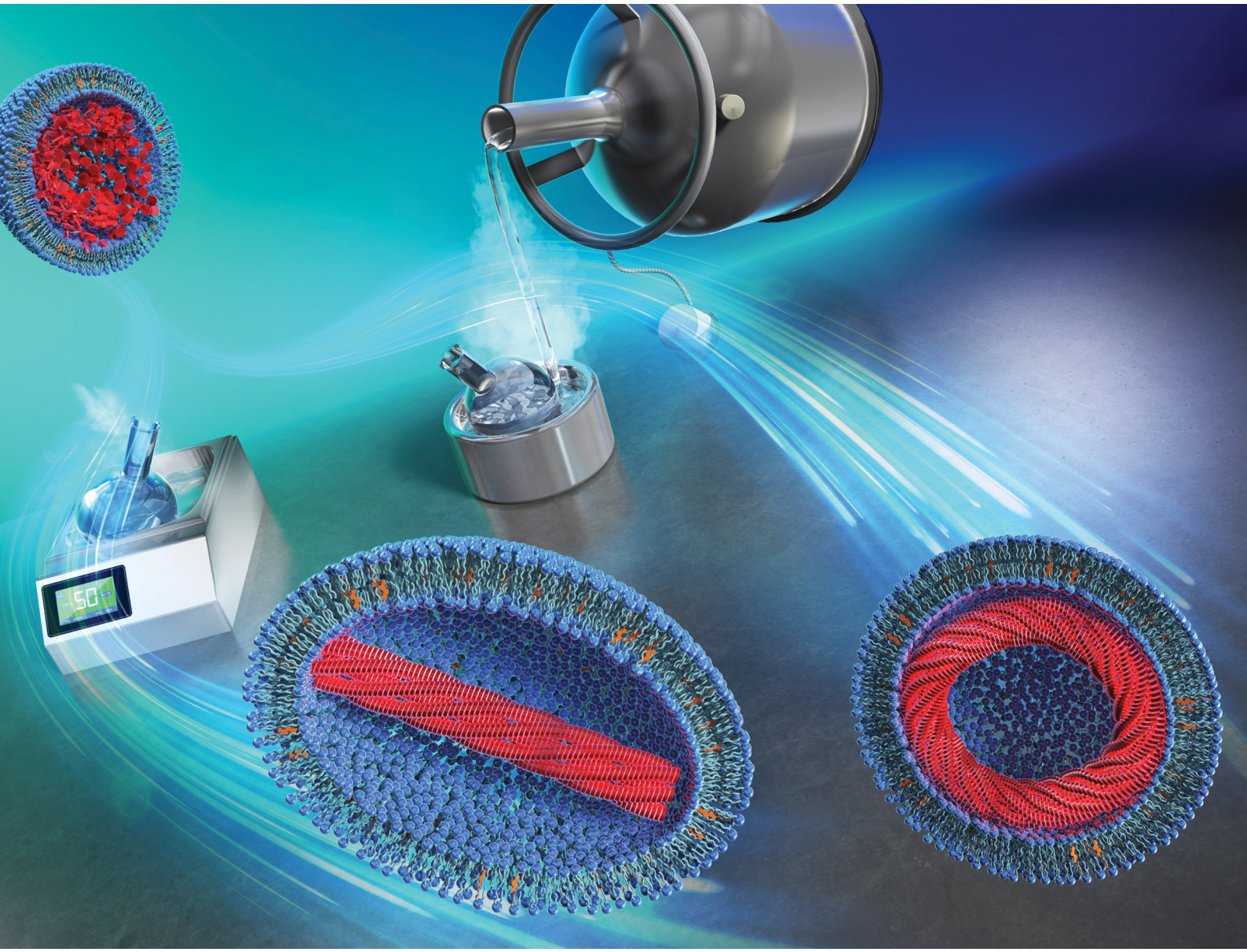

ISSN 1359-7345

ROYAL SOCIETY OF CHEMISTRY

COMMUNICATION

Kenjirou Higashi *et al.*

Nanomorphology tuning in doxorubicin-loaded liposomes *via* cooling-induced doxorubicin-crystallization and membrane phase transition

ChemComm

COMMUNICATION

View Article Online
View Journal | View Issue

Cite this: *Chem. Commun.*, 2025, 61, 9876

Received 30th April 2025,
Accepted 22nd May 2025

DOI: 10.1039/d5cc02434j

rsc.li/chemcomm

Nanomorphology tuning in doxorubicin-loaded liposomes *via* cooling-induced doxorubicin-crystallization and membrane phase transition†

Koki Nishimura,‡[a] Taiki Fujimoto,‡[a] Taisei Tokumoto,‡[a] Kenjirou Higashi,*[a] Ryo Hidaka,[a] Keisuke Ueda,[a] Takeshi Morita[b] and Kunikazu Moribe[a]

Rational control of doxorubicin (DOX)-loaded liposome morphology was achieved by changing the cooling rate without altering the composition. Slow cooling produced prolate liposomes containing a linear DOX-sulfate fiber-bundle, whereas rapid freezing gave nearly spherical liposomes with a curved DOX-sulfate fiber-bundle. *In situ* SAXS and ^{1}H NMR measurements revealed that the morphological differences were determined by the sequence of DOX-sulfate fiber-bundle formation and stiffness increase of the lipid membrane, depending on the cooling rate.

The liposomal product Doxil®/Caelyx®, the first to load the anticancer drug doxorubicin (DOX, Fig. S1, ESI†), was approved by the U.S. Food and Drug Administration (FDA) in 1995.[1,2] Over the past thirty years, seven anticancer liposomal products have been approved, and more than ten are currently undergoing clinical trials.[3] Several generics of Doxil®/Caelyx® are already on the market, while multiple DOX-loaded liposomal formulations with enhanced functionality are in clinical trials. Due to its historical significance and continued relevance, the DOX-loaded liposome remains one of the most representative nanoparticles in drug delivery systems (DDSs).

The physical properties of nanoparticles, including size, morphology, charge, and surface coating, play a crucial role in determining their biodistribution after administration.[4] Evaluation of liposomal morphology is essential and has been included in draft guidelines and reflection papers by the FDA and the European Medicines Agency (EMA). Spherical liposomes can undergo deformation when crystalline drugs such as DOX,[5] topotecan,[6] and docetaxel[7] are loaded into their inner aqueous phase. In Doxil®/Caelyx®, the linear fiber-bundle formation of a DOX-sulfate liquid-crystal in the inner aqueous phase causes physical stretches of the lipid membrane, resulting in a well-known "coffee-bean" morphology.[8] Doxil®, Caelyx®, and their two generic products showed differences in complement activation in human sera, which are believed to be caused by morphological variations.[9] Modifying the composition, such as altering the loading buffer in the inner phase and the lipid/DOX ratio, can change the liposome morphology along with the DOX fiber-bundle size and shape and affect *in vitro* and *in vivo* release, cellular uptake, and toxicity in cancer cells.[10–12] TLD-1 (Talidox, Innomedica, Bern, Switzerland), a DOX-loaded formulation currently in a phase-II clinical trial, was designed with a smaller particle size than 70 nm and a reduced lipid/DOX ratio to prevent deformation and maintain a spherical shape.[13] In the present study, we obtained different DOX-loaded liposome morphologies by modifying the preparation conditions or controlling the cooling rate without altering the composition. Furthermore, the underlying mechanism was clarified by monitoring the DOX-sulfate and lipid membrane phase changes during the cooling process using *in situ* ^{1}H nuclear magnetic resonance (NMR) and small-angle X-ray scattering (SAXS) measurements.

Liposomes composed of HSPC/cholesterol (60 : 40 mol%) with an approximate size of 100 nm were prepared by lipid film hydration and extrusion processes (Scheme S1 and Fig. S2, ESI†). DOX was loaded using the active loading method. Fig. 1 presents the cryo-TEM images of liposomes after DOX loading at 10–30 mol% concentrations at 65 °C, followed by cooling at different rates. The encapsulation efficiency of DOX in each liposome was confirmed to exceed 90% (Table S1, ESI†). By slow cooling (cooled from 65 °C to 4 °C at 1 °C min^{-1}), a linear DOX-sulfate fiber-bundle accumulated within the inner aqueous phase. At 10 mol% loading, the liposome maintained a spherical shape, with negligible effect of DOX-loading. The fiber-bundle edges attached to the liposome membrane; however, the exerted force was insufficient to induce the membrane deformation because the fiber-bundle was still thin. In liposomes with 20 mol% DOX loading,

[a] *Graduate School of Pharmaceutical Sciences, Chiba University, 1-8-1 Inohana, Chuo-ku, Chiba 260-8675, Japan. E-mail: ken-h@faculty.chiba-u.jp*
[b] *Graduate School of Science, Chiba University, 1-33 Yayoi-cho, Inage-ku, Chiba 263-8522, Japan*

† Electronic supplementary information (ESI) available. See DOI: https://doi.org/10.1039/d5cc02434j

‡ These authors contributed to this work equally.

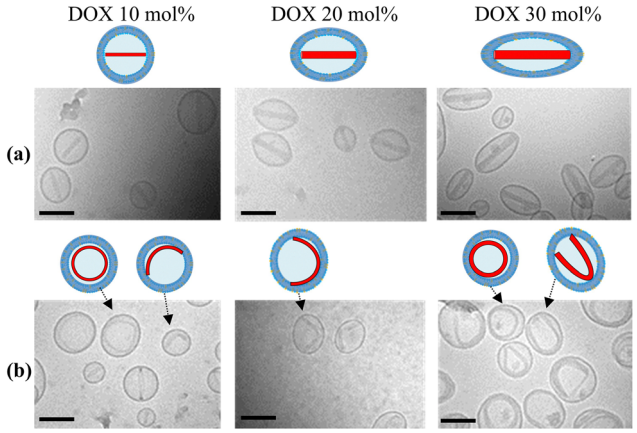

Fig. 1 Cryo-TEM images of DOX-loaded liposomes (10–30 mol%) prepared with (a) slow cooling (65 °C to 4 °C at 1 °C min^{-1}) and (b) rapid freezing (65 °C to −196 °C with liquid nitrogen and re-heated to 4 °C). Each bar represents 100 nm.

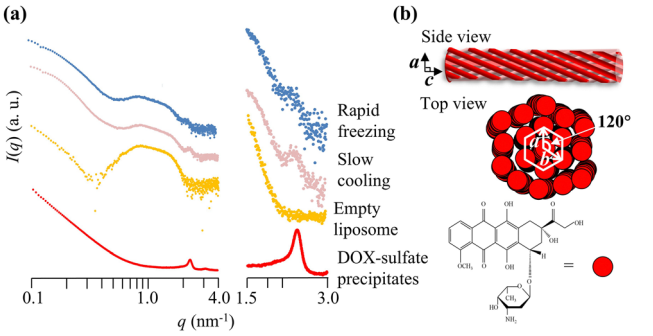

Fig. 2 (a) SAXS profiles at 25 °C in the full (q = 0.1–4.0 nm^{-1}) and expanded (q = 1.5–3.0 nm^{-1}) region and (b) schematic representation of a DOX-sulfate fiber-bundle with 3D hexagonal lattice: $a = b$ = 3.18 nm and c = 2.02 nm. The scattering parameter q is defined by $4\pi \sin\theta/\lambda$ (2θ, scattering angle; λ, the wavelength of X-rays).

the fiber-bundle thickened and deformed the liposome, corresponding to the characteristic "coffee-bean" morphology. DOX crystallization primarily contributed to thickening the fiber-bundle, because the lipid membrane restricted linear elongation. However, elongation was not entirely suppressed because the increased force exerted by the thickened fiber-bundle allowed for membrane extension, which deformed the liposome morphology. Fiber-bundle thickening was even more pronounced at 30 mol% DOX loading, resulting in a prolate-shaped liposome.

In contrast, by the rapid freezing process (cooled from 65 °C to −196 °C by liquid nitrogen and re-heated to 4 °C), spherical liposomes containing a curved fiber-bundle (ring- and U-shape) accounted for the vast majority. Considering that a DOX fiber-bundle forms a linear strained morphology in bulk water,[5] the curved fiber-bundle was specifically formed within the nano-confined space of the liposomal inner phase. This morphology transformation of the DOX fiber-bundle within the liposome can be regarded as one of the cell-size space effect (CSE), where the characteristics and phase transition of nucleic acids, proteins, and polymers confined in a microscopic space often differ from their bulk-state behavior.[14,15] At 10 mol% DOX loading, the curved fiber-bundles containing ring- and U-shaped ones remained thin and did not deform the lipid membrane, allowing the liposome to retain its spherical shape. Even with increased DOX loading to 20 and 30 mol%, the thickened ring-shaped fiber-bundles did not deform the liposomes. The ends of the fiber-bundle fused to form enclosed rings and prevented direct contact with the lipid membrane. The thickening of the U-shaped fiber-bundle exerted force on the lipid membrane by pushing the lipid membrane with the attached edges of the fiber-bundle. This induced the transition of the liposome morphology from spherical to oblate, although the deformation was much suppressed compared with prolate liposomes prepared with slow cooling. By the fast cooling process (cooled from 65 °C to 4 °C by water bath at 4 °C, Fig. S3a, ESI†), which uses an intermediate cooling rate between slow cooling and rapid freezing, a mixture of spherical liposomes containing a curved fiber-bundle and prolate liposomes containing a linear fiber-bundle was observed. These results show that increasing the cooling rate reduces the fraction of typical linear-bundle liposomes while increasing the unique curved-bundle liposomes.

The DOX-loaded liposomes (30 mol%) prepared under different cooling rates were evaluated using SAXS measurement at 25 °C (Fig. 2). DOX-sulfate precipitates prepared in bulk water (Scheme S2, ESI†) exhibited a Bragg peak at q = 2.3 nm^{-1}. This peak corresponds to the (hkl) = (100) peak of a three-dimensional hexagonal lattice of the DOX-sulfate liquid-crystal, with unit cell dimensions of $a = b$ = 3.18 nm and c = 2.02 nm[16] (Fig. 2b). The peak intensity was considerably lower for the rapid freezing than the slow cooling. The lower peak intensity could be attributed to the transformation of fiber-bundles from a linear to a curved shape. The primary mechanism should be a decrease in the crystallinity of the DOX-sulfate liquid-crystal. The arrangement of DOX molecules in the fiber-bundle could be disordered by bending, and the curved fiber-bundle resulted in lowered peak intensity compared to a linear fiber-bundle. Another possible mechanism is a difference in the crystal habit. A thinner, longer fiber-bundle reduced the peak intensity at q = 2.3 nm^{-1}, given the fewer (100) faces in the hexagonal lattice. Since the curved fiber-bundle was thinner and longer than linear ones formed in the confined liposomal inner space, this difference could also contribute to the observed lower peak intensity.

In situ SAXS measurements were conducted to understand the formation process of linear-bundle liposomes during slow cooling (Fig. 3). The profile before incubation (yellow) almost coincided with that of empty liposomes. During the incubation at 65 °C (red), the peak intensity in the range of q = 0.1–0.4 nm^{-1} and 2.0–4.0 nm^{-1} increased rapidly, which could be due to the rapid loading of DOX into the liposomal inner phase. No Bragg peaks were detected, suggesting that the loaded DOX was in a non-crystalline state. During the subsequent slow cooling process at 1 °C min^{-1} (blue), the scattering intensity around q = 0.1–0.4 nm^{-1} increased, while that around q = 1.0–4.0 nm^{-1} decreased. Additionally, a Bragg peak at q = 2.3 nm^{-1} appeared. These changes reflected the fiber-bundle formation

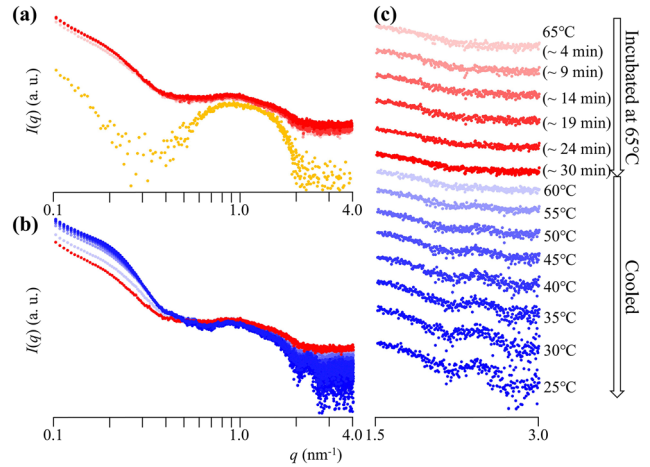

Fig. 3 Overlapped *in situ* SAXS profiles (q = 0.1–4.0 nm^{-1}) during (a) incubation at 65 °C for 30 min and (b) cooling from 65 °C to 25 °C at the rate of 1 °C min^{-1}. The yellow profile before incubation, which is a mixture of empty liposomes and DOX-HCl solution at 25 °C, is also shown in (a). (c) Enlarged view (q = 1.5–3.0 nm^{-1}) of (a) and (b) combined.

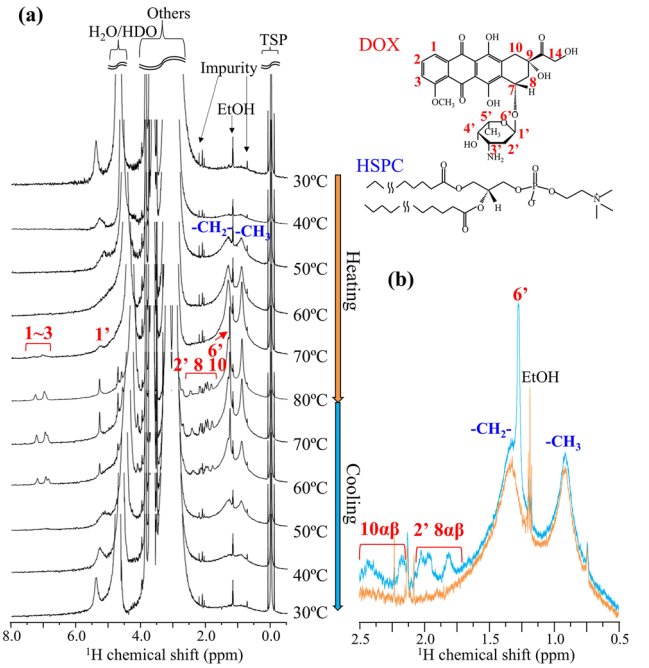

Fig. 4 (a) *In situ* ^{1}H NMR spectra during heating and cooling processes of DOX-loaded liposomes (30 mol%) prepared with slow cooling and (b) enlarged spectra of 60 °C during (orange) heating and (blue) cooling processes.

by crystallization of DOX-sulfate. The changes became more pronounced upon further cooling to 25 °C. Notably, drastic changes were observed between 65–50 °C, indicating that fiber-bundle formation predominantly occurred within this temperature range.

To evaluate the molecular-state changes in both the fiber-bundle of DOX-sulfate and the liposomal membrane of the lipid, *in situ* ^{1}H NMR measurements were conducted during the heating and cooling processes for the DOX-loaded liposomes (30 mol%) prepared *via* the slow cooling process (Fig. 4). First, we examine the changes in DOX peaks (shown in red). During heating, no DOX peaks were detected below 60 °C. The peaks were too broad to be detected due to strong ^{1}H–^{1}H homonuclear dipole interaction because DOX-sulfate could have low molecular mobility in a liquid-crystalline fiber-bundle. DOX peaks began to appear at 70 °C and sharpened at 80 °C, reflecting its enhanced molecular mobility. In the differential scanning calorimetry (DSC) profile of DOX-sulfate precipitates in bulk water (Fig. S4a, ESI†), the melting started around 60 °C and was completed below 80 °C. Similarly, DOX-sulfate liquid crystals within the liposomal inner phase could melt between 60–80 °C. To further understand the molecular state of DOX-sulfate in the inner phase, its ^{1}H NMR spectrum at 70 °C was compared with that of DOX-HCl dissolved in bulk water (Fig. S5, ESI†). The peaks of DOX-sulfate in the inner phase appeared at a higher magnetic field, especially for aromatic peaks, and exhibited broader shapes. Concentrated DOX molecules in the confined inner phase could interact with each other through π–π stacking interactions,[17] and the mobility was suppressed, although it could exist in a liquid state. During cooling, DOX-sulfate peaks disappeared at 50 °C, indicating the recrystallization into liquid-crystalline fiber-bundles. Notably, the peak intensities of DOX-sulfate at 60 °C and 70 °C during cooling were higher than those at the same temperature during heating. The representative spectra at 60 °C for heating and cooling are shown in Fig. 4b. These results indicate that, even at a slow cooling rate of 1 °C min^{-1}, some DOX-sulfate did not recrystallize at these temperatures and remain in a supercooled-liquid state. This can be further supported by the DSC results of DOX-sulfate precipitates prepared in bulk water (Fig. S4, ESI†), where the temperature of DOX-sulfate crystallization was dependent on the cooling rate. These results show that the fiber-bundle formation *via* DOX-sulfate crystallization during cooling occurs at the minute scale or slower.

Secondly, the peak changes in lipid acyl chains within the liposomal membrane (shown in blue) were analyzed.[18] During heating, the peak intensity around 0.9 and 1.3 ppm increased with noticeable peak sharpening. The sharpening was particularly pronounced around 50 °C close to the HSPC transition temperature of solid-ordered phase (s_o) to liquid-disordered phase (l_d) at 53.6 °C.[19,20] Previous studies have reported that acyl chains within the cholesterol-rich phase or the liquid-ordered (l_o) phase exhibited broad transitions centered around the phase transition temperature of pure phospholipids.[21] Thus, the enhanced mobility of acyl chains in the HSPC/cholesterol membrane upon heating could occur around 50 °C with a broad temperature range. During cooling, the peak intensity decreased, accompanied by peak broadening. Notably, almost no significant thermal hysteresis was observed; the peak shapes of the lipid acyl chains remained consistent at equivalent temperatures during heating and cooling (represented as Fig. 4b). This suggests that, in slow cooling of 1 °C min^{-1}, the lipid membrane rapidly reached its energetic equilibrium state at each temperature. Previous papers supported this observation, showing that the lipid membrane transition of DSPC, a main component of HSPC, occurs within a timescale of seconds.[22]

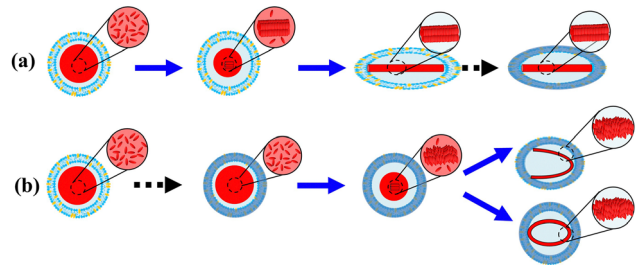

Fig. 5 A proposed mechanism of the morphological change of DOX-loaded liposomes prepared with (a) slow cooling and (b) rapid freezing. The solid blue arrow shows the fiber-bundle formation and elongation *via* DOX-sulfate crystallization, while the dotted black arrow indicates the stiffness increase by phase transition of the lipid membrane.

Based on the results above, a mechanism of morphological change of DOX-loaded liposomes as a function of cooling rate is proposed (Fig. 5). The sequence of DOX-sulfate fiber-bundle formation *via* crystallization and stiffness increase of the lipid membrane *via* phase transition could determine the final morphology. DOX was loaded into the liposomal inner phase at 65 °C *via* an ionic ammonium sulfate gradient, forming DOX-sulfate. Given its highly concentrated state and melting temperature range (60–80 °C), DOX-sulfate could exist as either a liquid or supercooled-liquid state. The DOX-sulfate crystallized into a liquid-crystalline fiber-bundle during the cooling process. In bulk water, the DOX fiber-bundle exhibited a string-like morphology,[5] which can be explained by its preferential crystallization along the *c*-axis (elongation) rather than the *a* and *b* axis (thickening). Similarly, the DOX-sulfate fiber-bundle in the liposome inner phase could begin to elongate. However, elongation was hindered when the fiber-bundle edges were attached to the inner leaf of the lipid membrane. When the cooling rate was slow (Fig. 5a), most DOX-sulfate formed rigid liquid-crystalline fiber-bundles mainly between 65–50 °C, before the liposomal membrane increased the stiffness around the phase transition temperature of 53.6 °C. The fiber-bundle could solidify linearly, gradually extending the soft liposomal membrane, ultimately producing a prolate liposome containing linear fiber-bundles. In contrast, when the cooling rate was relatively high in the rapid freezing process (Fig. 5b), the sequence of DOX-sulfate fiber-bundle formation and the stiffness increase of the liposomal membrane were reversed. Immediately after cooling, DOX-sulfate temporarily existed as a supercooled-liquid state because its crystallization occurs on a minutes scale or slower. Meanwhile, the lipid membrane rapidly reached thermal equilibrium due to its second-scale phase transition. Thus, the stiffness of the lipid membrane formerly increased, and a rigid spherical liposome was formed. The steric hindrance of the rigid lipid membrane prevents DOX-sulfate from crystallizing in a linear direction, instead forming curved bundles with a less ordered arrangement of DOX-sulfate (suggested in Fig. 2). The formation of DOX-sulfate fiber-bundles and the stiffness increase of the liposomal membrane occurred competitively during fast cooling with an intermediate cooling rate. As a result, a mixed population of linear-bundle liposomes and curved-bundle liposomes are observed (Fig. S3b, ESI†).

In summary, we have found that the morphology of DOX-loaded liposomes can be precisely controlled solely by changing the cooling rate after DOX loading. Specifically, the curved-bundle liposomes containing ring- and U-shaped DOX-sulfate fiber-bundles, whose deformation was much suppressed compared with typical linear-bundle liposomes, were selectively obtained with a rapid cooling rate. Furthermore, we identified that the sequence of DOX-sulfate fiber-bundle formation (occurring on a minute-scale or slower) and the stiffness increase of the lipid membrane (occurring on a second scale) during cooling governs the final morphology of the DOX-loaded liposome. This finding helps in designing liposomal formulations other than DOX-loaded liposomes.

This work was financially supported in part by JSPS KAKENHI (Grant No. 24K02162). The synchrotron SAXS measurements were carried out on BL-10C at the Photon Factory (Proposal No. 2019G532, 2021G562, and 2023G596).

Data availability

The data supporting this article have been included as part of the ESI.†

Conflicts of interest

There are no conflicts to declare.

Notes and references

1 B. S. Pattni, *et al.*, *Chem. Rev.*, 2015, **115**, 10938–10966.
2 M. Biscaia-Caleiras, *et al.*, *J. Controlled Release*, 2024, **373**, 617–639.
3 A. G. Alberto, *et al.*, *BMJ Oncol.*, 2025, **4**, e000573.
4 R. Tenchov, *et al.*, *ACS Nano*, 2021, **15**, 16982–17015.
5 X. Li, *et al.*, *Biochim. Biophys. Acta, Biomembr.*, 1998, **1415**, 23–40.
6 D. Zucker and Y. Barenholz, *J. Controlled Release*, 2010, **146**, 326–333.
7 I. V. Zhigaltsev, *et al.*, *J. Controlled Release*, 2010, **144**, 332–340.
8 D. D. Lasic, *et al.*, *FEBS Lett.*, 1992, **312**, 255–258.
9 P. P. Wibroe, *et al.*, *J. Controlled Release*, 2016, **221**, 1–8.
10 Y. Schilt, *et al.*, *Biochim. Biophys. Acta, Gen. Subj.*, 1865, **2021**, 129849.
11 A. Ruiz, *et al.*, *J. Controlled Release*, 2020, **328**, 665–678.
12 N. Takahashi, *et al.*, *J. Pharm. Sci.*, 2018, **107**, 717–726.
13 K. Gan, *et al.*, *Int. J. Pharm.*, 2024, **654**, 123942.
14 M. Yanagisawa, *et al.*, *Langmuir*, 2022, **38**, 11811–11827.
15 T. Litschel, *et al.*, *Nat. Commun.*, 2021, **12**, 2254.
16 Y. Schilt, *et al.*, *Biochim. Biophys. Acta, Gen. Subj.*, 1860, **2016**, 108–119.
17 W.-R. Zhuang, *et al.*, *J. Controlled Release*, 2019, **294**, 311–326.
18 N. Maurer, *et al.*, *Biochim. Biophys. Acta, Biomembr.*, 1998, **1374**, 9–20.
19 H. Kitayama, *et al.*, *Chem. Pharm. Bull.*, 2014, **62**, 58–63.
20 D. Marsh, *Biochim. Biophys. Acta, Biomembr.*, 2010, **1798**, 688–699.
21 J. A. Clarke, *et al.*, *Biophys. J.*, 2006, **90**, 2383–2393.
22 M. Schiewek and A. Blume, *Eur. Biophys. J.*, 2010, **39**, 815–824.